

Received December 6, 2020, accepted December 28, 2020, date of publication January 8, 2021, date of current version January 20, 2021.

Digital Object Identifier 10.1109/ACCESS.2021.3050186

An Enhanced Hemostatic Ultrasonic Scalpel Based on the Longitudinal-Torsional Vibration Mode

JINHUA LI¹, (Member, IEEE), XINYU DONG¹, GUANGHAO ZHANG¹, ZHICHENG GUO¹,
GUOKAI ZHANG², AND CHAOYANG SHI¹, (Member, IEEE)

¹Key Laboratory of Mechanism Theory and Equipment Design, Ministry of Education, School of Mechanical Engineering, Tianjin University, Tianjin 300072, China

²Department of Informatics, King's College London, London SE1 7EU, U.K.

Corresponding author: Chaoyang Shi (chaoyang.shi@tju.edu.cn)


This work was supported in part by the National Key R&D Program of China under Grant 2017YFC0110401 and Grant 51520105006, and in part by the EPSRC LoCoMoTE Project under Grant EP/R013977/1.

ABSTRACT This paper proposes an ultrasonic scalpel based on the longitudinal-torsional vibration mode to enhance the hemostatic ability. The concentrator of the proposed ultrasonic scalpel has been specially designed with spiral grooves to realize this vibration mode. The change of the working mode has enlarged the vertical motion component of the distal blade to efficiently radiate energy into the dissected tissues, supporting that the blood vessel can receive sufficient energy to be sealed. The electromechanical equivalent method has been employed in the initial design of the scalpel to obtain the desired resonance frequency. The structural optimization based on the finite element method (FEM) has been conducted to further improve the proposed design, as well as investigation of its dynamic performances. Both the conventional and presented ultrasonic scalpel prototypes were fabricated, and their important parameters such as, mechanical quality factor and resonance frequency, were tested and compared using an impedance analyzer. The ex-vivo experiments have been conducted to measure the vertical temperature distribution to investigate their transferring heat effects. The corresponding results indicated that the internal temperature values of tissues cut with the proposed hemostatic-enhanced ultrasonic scalpel are 24.0% higher on the 3mm layer, 16.5% higher on the 6mm layer, and 8.5% higher on the 9mm layer, respectively. The sealing capacity of the ultrasonic scalpels has been investigated through the coagulation dissection experiment on the chicken carotid and their burst pressure tests. The average burst pressure of the sealed vessels by the hemostatic-enhanced ultrasonic scalpel can achieve higher values than that of the conventional ultrasonic scalpel.

INDEX TERMS Electrosurgery, ultrasonic scalpel, enhanced hemostatic, design optimization, piezoelectric ceramics.

I. INTRODUCTION

Ultrasonic scalpels have been increasingly introduced as a kind of preferred energy-based surgical instrument to perform precise dissection of soft tissues in a variety of clinic procedures [1]–[3]. They can offer significant advantages over the traditional electrosurgery devices in terms of greater cutting precision, less toxic surgical smoke [4], and avoidance of potential safety hazards such as unintended burns to the patient and malfunction of implanted electronic devices (pacemakers or cardioversion devices etc.) [5]. The ultrasonic scalpel is typically composed of a piezoelectric converter,

The associate editor coordinating the review of this manuscript and approving it for publication was Jingang Jiang .

a flange, a concentrator, and a blade, as shown in Fig. 1. The piezoelectric ceramic is an outstanding candidate for ultrasonic scalpel actuators due to its excellent performances in terms of rapid responses to voltage inputs, high stiffness and large output force [6]–[9]. Ultrasonic piezoelectric converters can transform the high-frequency ultrasonic oscillating signals into mechanical vibration based on the converse piezoelectric effect [10], [11]. The concentrator is designed to focus the mechanical vibration energy and amplify the vibration amplitude generated by the piezoelectric converter. The amplified vibration eventually transmits to the distal blade. With the high-frequency vibration of the blade, fracture occurs within the tissue and the heat generated by the oscillation can cause protein coagulation during the

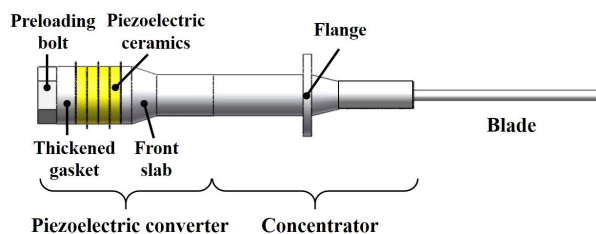


FIGURE 1. Schematic structure of the typical ultrasonic scalpel.

tissue-tool interaction, allowing for simultaneous cutting and sealing.

However, the existing ultrasonic scalpels are not competent in all situations. Previous studies indicated that the conventional ultrasonic scalpels typically generate a temperature below $80\sim 100^{\circ}\text{C}$ while cutting, which is not capable of sealing the vessels with a large diameter of more than 3mm [12]–[14]. To avoid the rupture of large blood vessels and the possibly serious surgical risks, instead of the energy-based hemostatic instruments, vascular closure devices [15], titanium nip [5], and staplers [16] are often selected as hemostatic tools. Nevertheless, these methods will leave foreign substances in the human body and the frequent replacement of surgical instruments will extend the operation time and lead to increased risks of surgical complications. Ethicon has developed a novel hemostatic ultrasonic scalpel (Harmonic Ace, Ethicon, USA), which can seal thick blood vessels by decreasing the input power while cutting to extend coagulation time [17], but its longer coagulation time enormously increases thermal damage [18]. BOWA has proposed a novel scalpel to perform the dissection by pure torsional oscillation (LOUTS, BOWA MEDICAL, UK), however, this scalpel also suffered from aggravated thermal damage [19]. Olympus has combined the advantages of both the ultrasonic scalpel and the bipolar electrosurgical scalpel (Thunderbeat, Olympus, Japan) to achieve the task of sealing 7mm-diameter blood vessels [20]. However, the introduction of the electrosurgical method makes the system complicated and could bring potential safety risks. Many studies have been performed to optimize the ultrasonic scalpel design. Ogura *et al.* [21] developed a bendable ultrasonic scalpel using a superelastic nickel-titanium alloy blade, but the vibration amplitude suffered from a decrease of 42% when operating in the bent state, which weakens the cutting performance. Khalaji *et al.* [22] developed a 3-DOF wrist-articulated ultrasonic scalpel that enables bending and deflecting motion of the scalpel by miniaturizing the scalpel and integrating it into an end-effector based on a double-parallellogram structure. These designs focus on enhancing the flexibility and mobility of the ultrasonic scalpel instead of improving the hemostatic properties of the ultrasonic scalpel. Using the surgical-grade stainless steel and silicon, Kuang *et al.* [23] developed a new type of ultrasonic scalpel that was configured as a flat shape for the main body and worked with a lateral vibration mode. However, this design suffered from problems in terms of easy

cracking under high-stress conditions and significant heat generation phenomena. To enhance the hemostatic capacity and expand the application scenarios, an enhanced hemostatic ultrasonic scalpel is required.

When sealing the larger arteries, an appropriate increase in heat generation is essential. K. Ebina *et al.* have validated that the heat generation in the duration of dissection is mainly caused by the tissue's expansion and contraction, instead of the friction between the scalpel and tissue, by carrying out an experiment with an ultrasonic scalpel under a 44.3kHz driving signal. This indicates that a vertical rather than a longitudinal vibration can generate more heat to coagulate the deeper tissue [24]. As the torsional vibration has a larger vertical motion component and can radiate more energy in the lateral direction, it can be inferred that the introduction of torsional vibration mode into longitudinal mode will enhance the capacity of sealing large arteries.

Based on the above analysis, the mechanical structure of the concentrator on the enhanced hemostatic ultrasonic scalpel has been designed with spiral grooves. It can be driven by the piezoelectric ceramics to change the operating mode from the longitudinal vibration to longitudinal-torsional vibration. With the introduction of this torsional vibration, the vertical motion component is significantly enlarged, thus transferring energy more efficiently into the tissues and improving the sealing capacity. This paper is organized as follows. Section 2 illustrates the initial mechanical design of the scalpel. In Section 3, the finite element method (FEM)-based simulation and structural optimization have been performed to investigate and enhance the cutting and sealing performances. The measurements of the performance parameters of the proposed enhanced hemostatic ultrasonic scalpel and the conventional ultrasonic scalpel have been conducted in Section 4, as well as two kinds of ex-vivo tissue experiments for design verification and comparison. The conclusion part has been presented in Section 5.

II. MECHANICAL DESIGN OF THE HEMOSTATIC ULTRASONIC SCALPEL

To achieve an excellent cutting and sealing performance, the ultrasonic scalpel typically works under the resonance frequency to efficiently transfer more energy. Recent studies have validated and suggested that the typical resonance frequency values of around 55kHz and 55.5kHz for the ultrasonic scalpel can better achieve such an aim through a series of experiments [2], [25]. Therefore, the initial structure design of the scalpel in this work is targeted at a resonance frequency of 55.5 kHz.

A. INITIAL STRUCTURAL DESIGN OF ULTRASONIC SCALPEL

The ultrasonic scalpel consists of a preloading bolt, a thickened gasket, a stack of piezoelectric ceramics, a front slab, a concentrator, and a scalpel blade, as shown in Fig. 1. Four pieces of the ring-shaped piezoelectric ceramics (C-213, Fujicera, Japan) are stacked and integrated to drive

TABLE 1. Material parameters of each component of the scalpel.

Parameters	BAG	PZT	Concentrator	Blade
Material	304	PZT-8	7075	TC4-ELI
Density (kg/m ³)	7930	7800	2810	4470
Young's modulus (GPa)	193	--	71	110
Poisson ratio	0.29	--	0.33	0.32
Acoustic impedance (10 ⁵ Pa · s/m ³)	44.6	26.2	16.9	28

the designed ultrasonic scalpel to provide sufficient cutting energy.

The uniform prestress of about 25MPa is applied onto the gasket attached with the piezoelectric ceramics by using the preloading bolt, to guarantee the full contact among different components. This prestress can also suppress the PZT hysteresis phenomenon so as to provide improved output performances. In order to enhance the transmission efficiency of ultrasonic energy from the proximal piezoelectric ceramics to the distal blade, the material selected for the ultrasonic scalpel needs to comply with the following rules of acoustic impedance [26].

$$\begin{cases} Z_{BAG} > Z_{PZT} > Z_{con} \\ Z_{PZT} = \sqrt{Z_{con} * Z_{BAG}} \end{cases} \quad (1)$$

where, Z_{PZT} and Z_{con} represent the acoustic impedance of the piezoelectric ceramic and the concentrator respectively. Z_{BAG} denotes the combined acoustic impedance of the bolt and gasket. According to the parameter comparison of the standard medical materials, the materials for each component have been selected and summarized in Table. 1. In particular, the TC4 titanium alloy has been selected for the blade fabrication to provide a long service life and an excellent cutting performance, due to its excellent attributes of low acoustic impedance, high tensile strength, and light weight [27].

To obtain the desired resonance frequency, the electromechanical equivalent method has been employed to establish the equation of structural dimensions and resonance frequency [26], [28], [29]. Since there are similarities between the mechanical vibration and electrical resonance, we can equate the typical parameters of mass or vibration speed with electrical counterpart quantities based on the electromechanical equivalent method to form an electromechanical equivalent circuitry, as shown in Fig. 2. Z_x denotes the equivalent impedances corresponding to each component of the ultrasonic scalpel; U expresses the voltage applied to the scalpel; C_0 represents the one-dimensional cut-off capacitance of the piezoelectric ceramic stack; P is the number of the piezoelectric ceramics, and n is the electromechanical coefficient of the ceramics.

According to Kirchhoff's law, the total impedance can be determined as follows.

$$Z_{total} = \frac{Z_{elec} n^2 Z_m}{Z_{elec} + n^2 Z_m} = \text{Re}(Z_{total}) + \text{Im}(Z_{total}) \quad (2)$$

where

$$Z_{elec} = \frac{1}{j\omega P C_0} \quad (3)$$

$$n = \frac{d_{33} S_e}{S_{33}^E \cdot t} \quad (4)$$

$$C_0 = \frac{\epsilon_{33}^S}{t} S_e \quad (5)$$

and

$$\begin{cases} Z_m = Z_{23} + \frac{(Z_{21} + Z_r)(Z_{22} + Z_s)}{(Z_{21} + Z_r) + (Z_{22} + Z_s)} \\ Z_r = Z_{12} + \frac{Z_{11} Z_{33}}{Z_{11} + Z_{33}} \\ Z_s = Z_{31} + \frac{(Z_{32} + Z_{41} + Z_{4f}) Z_{33}}{(Z_{32} + Z_{41} + Z_{4f}) + Z_{33}} \\ Z_{4f} = \frac{(Z_{42} + Z_{51} + Z_{5f}) Z_{43}}{(Z_{42} + Z_{51} + Z_{5f}) + Z_{43}} \\ Z_{5f} = \frac{(Z_{52} + Z_{61} + Z_{6f}) Z_{53}}{(Z_{52} + Z_{61} + Z_{6f}) + Z_{53}} \\ Z_{6f} = \frac{(Z_{62} + Z_{71} + Z_{7f}) Z_{63}}{(Z_{62} + Z_{71} + Z_{7f}) + Z_{63}} \\ Z_{7f} = \frac{(Z_{72} + Z_{81} + Z_{8f}) Z_{73}}{(Z_{72} + Z_{81} + Z_{8f}) + Z_{73}} \\ Z_{8f} = \frac{Z_{82} Z_{83}}{Z_{82} + Z_{83}} \end{cases} \quad (6)$$

where, S_e denotes the cross-sectional area of the PZT; t is the thickness of one piece PZT; d_{33} , S_{33}^E and ϵ_{33}^S represent the piezoelectric strain constant, elastic compliance constant and dielectric constant, respectively.

For each component, the impedance values can be calculated by

$$\begin{cases} Z_{i1} = j\rho_i c_i S_i \tan\left(\frac{k_i L_i}{2}\right) \\ Z_{i2} = Z_{i1} \\ Z_{i3} = \frac{\rho_i c_i S_i}{j \sin(k_i L_i)} \end{cases}, i = 1, 2, 3, 5, 6, 8 \quad (7)$$

$$\begin{cases} Z_{i1} = \frac{-j\rho_i c_i S_{i1}}{k_i L_i} \left(\sqrt{\frac{S_{i2}}{S_{i1}}} - 1 \right) - j\rho_i c_i S_{i1} \cot(k_i L_i) + \frac{j\rho_i c_i \sqrt{S_{i1} S_{i2}}}{\sin k_i L_i} \\ Z_{i2} = \frac{-j\rho_i c_i S_{i2}}{k_i L_i} \left(\sqrt{\frac{S_{i1}}{S_{i2}}} - 1 \right) - j\rho_i c_i S_{i2} \cot(k_i L_i) + \frac{j\rho_i c_i \sqrt{S_{i1} S_{i2}}}{\sin k_i L_i} \\ Z_{i3} = \frac{\rho_i c_i \sqrt{S_{i1} S_{i2}}}{j \sin k_i L_i} \end{cases}, i = 4, 7 \quad (8)$$

where, k_i is the wavenumber and it can be formulated as $k_i = \omega/c_i$; c_i stands for the wave speed; ρ_i is the density of each component of the scalpel; L_i and S_i denote the length and cross-sectional area of each component.

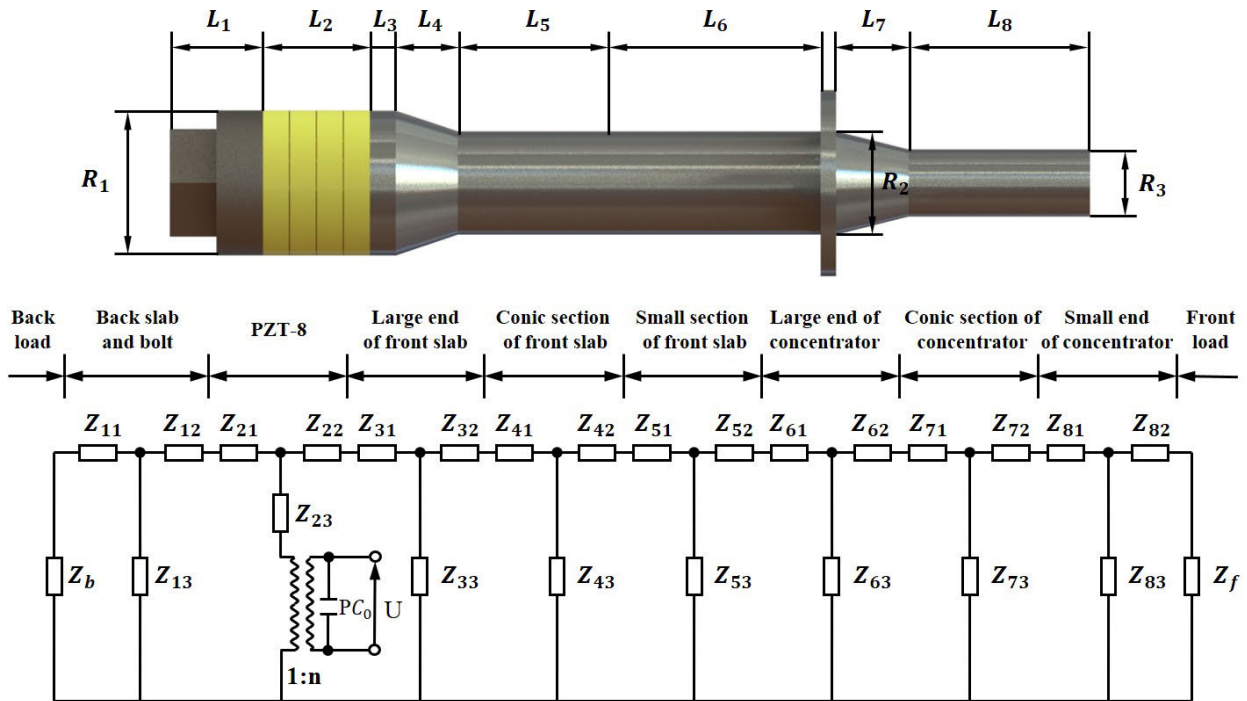


FIGURE 2. Electromechanical equivalent circuitry of the ultrasonic transducer.

When the ultrasonic scalpel is working under a resonant frequency, that is $Im(Z_{total}) = 0$, the dimensional parameters of the ultrasonic scalpel are derived based on the equations and comprehensive consideration of machining capacity and engineering experience, as labeled in Fig. 3

B. STRUCTURAL DESIGN OF THE ENHANCED HEMOSTATIC ULTRASONIC SCALPEL

To enhance the ultrasonic scalpel’s sealing capacity on the blood vessels with a large diameter, the improvement on the initial ultrasonic scalpel has been implemented by fabricating four spiral grooves on the concentrator. The detailed structure of the improved concentrator has been illustrated in Fig. 4. This structural modification can degenerate its working mode from the longitudinal vibration mode to the longitudinal-torsional vibration mode to increase the vertical motion component [30], thus improving the sealing capacity. The approach has been validated in the research fields of ultrasonic rock drilling devices and design of bone biopsy needles [30], [31]. The parameters of the improved concentrator include length L_6, L_7 and L_8 , width W , depth H , and spiral angle θ . The spiral angle θ could be obtained as follows:

$$\tan \theta = \frac{2\pi R}{L_8} \cdot \frac{\phi}{360} \tag{9}$$

where, ϕ denotes the rotation angle of the spiral groove. Considering the size limitation and machining capacity, the corresponding initial structure parameters of the concentrator are determined and summarized in Table. 2.

TABLE 2. Initial design parameters of the concentrator.

Key variables	Nomenclatures	Value(mm)
The length of the cylinder with a large diameter	L_6	21.5
The length of horn	L_7	7
The length of the spiral groove	L_8	15.5
The depth of the spiral groove	H	1
The width of the spiral groove	W	0.6
The rotation angle of the spiral groove	ϕ	360°

III. FEM SIMULATION-BASED DESIGN OPTIMIZATION OF THE HEMOSTATIC ULTRASONIC SCALPEL

After the calculation of the initial dimensions, the FEM-based design optimization has been carried out to further improve the cutting and sealing performances based on the ANSYS software (ANSYS18.0, ANSYS Inc, US).

A. FEM-BASED DESIGN OPTIMIZATION

The optimization process typically includes design variables, objective functions, a set of constraint functions, and the optimal solution. As the concentrator is the crucial part that transforms the longitudinal vibration mode to the longitudinal-torsional vibration mode, the following optimization will focus on its structural details. The optimization objective can be illustrated as enhancing the sealing capacity while maintaining the cutting performance. It can be achieved in three aspects. Firstly, to enhance the sealing capacity, the torsional-longitudinal vibration amplitude ratio should be

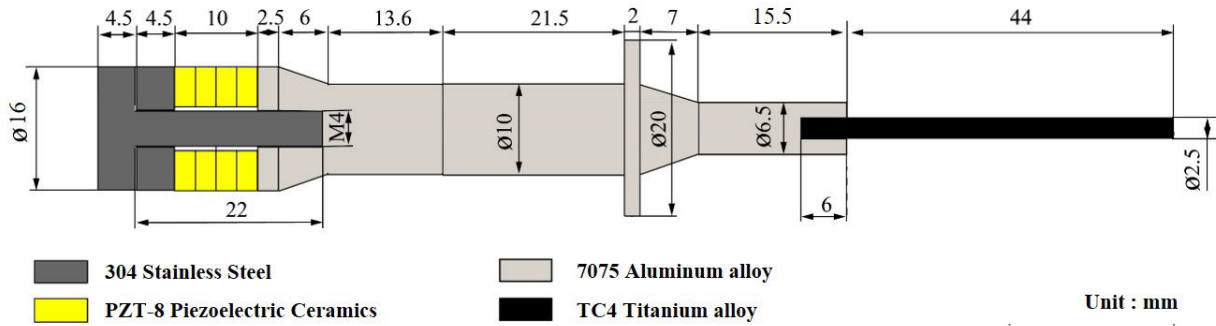


FIGURE 3. The initial dimensions of the designed ultrasonic scalpel.

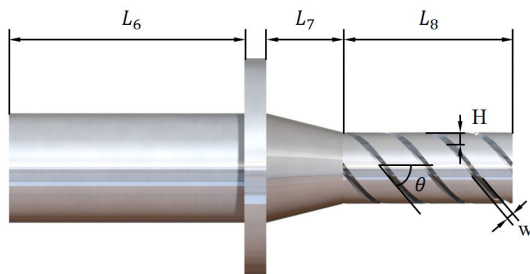


FIGURE 4. Key parameters of the improved concentrator.

increased to magnify the blade’s vertical motion component on the surface in contact with the tissue [24]. Secondly, to preserve the cutting performance, the resonance frequency should be consistent with the desired frequency. Thirdly, the ultrasonic transducer’s flange is connected to a fixed support, which may cause the coupled vibration between the ultrasonic scalpel and support. Therefore, the vibration amplitude of the flange should be minimized to avoid this coupling [32]. As mentioned above, the design optimization can be formulated as:

$$\text{Min} \left[|f - 55500|, |A_f|, \frac{1}{\left| \frac{A_t}{A_l} \right|} \right] \quad (10)$$

$$\text{s.t.} \begin{cases} 20\text{mm} \leq L_6 \leq 23\text{mm} \\ 6.5\text{mm} \leq L_7 \leq 7.5\text{mm} \\ 14.5\text{mm} \leq L_8 \leq 16.5\text{mm} \\ 0.4\text{mm} \leq W \leq 0.8\text{mm} \\ 300^\circ \leq \theta \leq 420^\circ \end{cases} \quad (11)$$

where, f denotes the resonance frequency of the scalpel; A_f is the vibration amplitude of the flange; A_t and A_l express the torsional and longitudinal vibration amplitude respectively. To ensure the working frequency is sufficiently close to the target resonance frequency of 55.5kHz, the variation ranges of the key variables should be limited to approach the resonance range, and they have also been determined with consideration of the machining capacity, as shown in (11).

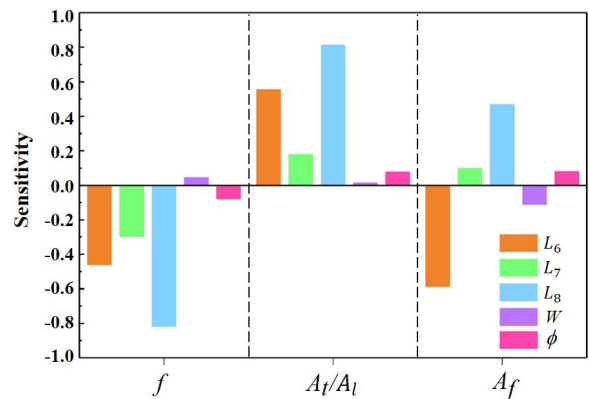


FIGURE 5. The contribution of the design variables on the objective functions based on sensitivity analysis.

To simplify the optimization process, unnecessary or unimportant variables should be ignored. Based on the built-in function block of Local Sensitivity in the ANSYS workbench software, the sensitivity analysis has been subsequently performed to analyze the contribution of each design variable on the results of objective functions, as illustrated in Fig. 5. The sensitivity value results vary in the range of $[-1, 1]$. Variables L_6 , L_7 and L_8 produce larger absolute values than the other variables, indicating more significant impacts on the objective functions. Thus, these three variables are selected as key variables to be optimized. The absolute sensitivity values of W and ϕ are much smaller (no more than 0.1 for each objective function), so they can be designed as constants to simplify the optimization process.

To reveal the relationship among the selected key design variables and the optimization objectives, the response surface methodology (RSM) has been adopted to generate response surfaces among the optimal objective and structural parameters [33]. The multi-objective genetic algorithm is a random search for algorithm with multiple start search points, which is well suitable to search the global optimal solution. Thus, it is subsequently utilized to determine the optimal value for each key variable based on the built-in functional block in ANSYS18.0.

TABLE 3. Key structural parameters and performance parameters before and after optimization.

Parameters	Initial Value	Optimal Value
$L_6(mm)$	21.5	22.68
$L_7(mm)$	7	6.51
$L_8(mm)$	15.5	15.7
$f(Hz)$	55586	55207
$ A_t/A_l $	31.1%	39.8%
$ A_f (\mu m)$	0.68	0.64

NODAL, SOLUTION

STEP=1

SUB =4

FREQ=55387

DMX =18.35

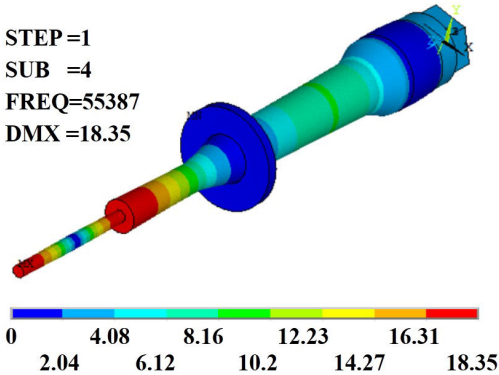


FIGURE 6. The deformation of the conventional ultrasonic scalpel in modal analysis.

The key structural parameters and performance parameters before and after optimization have been summarized and compared in Table 3. The ratio between the torsional vibration amplitude and longitudinal vibration amplitude of the proposed ultrasonic scalpel has increased from 31.1% to 39.8%, which indicates that the lateral radiation energy has been increased, as well as the sealing ability. The vibration amplitude of the flange has slightly decreased by 5.8%, which will result in a better decoupling capacity with the support. The resonance frequency has dropped only by 0.7%, and such a small change insufficiently affects the performances of the ultrasonic scalpel. So far, the dimensions of the ultrasonic scalpel have been finally determined.

B. FEM-BASED DYNAMIC PERFORMANCE INVESTIGATION

To validate the proposed enhanced hemostatic scalpel can generate a longitudinal-torsional vibration and radiate more energy than the conventional ultrasonic scalpel, the FEM-based simulation comparisons have been conducted between the ultrasonic scalpels with and without spiral grooves. The modal analysis on deformation distribution of these two scalpels has been conducted under the resonance frequency, as shown in Figs. 6 and 7. It can be inferred from the different deformation of the two scalpels that the torsional vibration has been generated and introduced into the primary longitudinal vibration mode. Moreover, the torsional displacement along the axis of the proposed enhanced hemostatic ultrasonic scalpel has been investigated through modal analysis, as shown in Fig. 8. The torsional displacement can

NODAL, SOLUTION

STEP=1

SUB =3

FREQ=55207

DMX =22.87

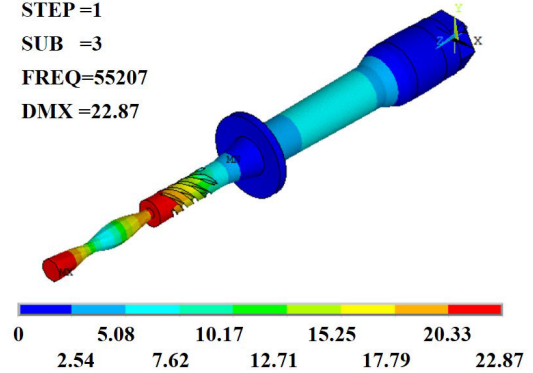


FIGURE 7. The deformation of the enhanced hemostatic ultrasonic scalpel in modal analysis.

NODAL, SOLUTION

STEP=1

SUB =3

FREQ=55207

DMX =-9.05

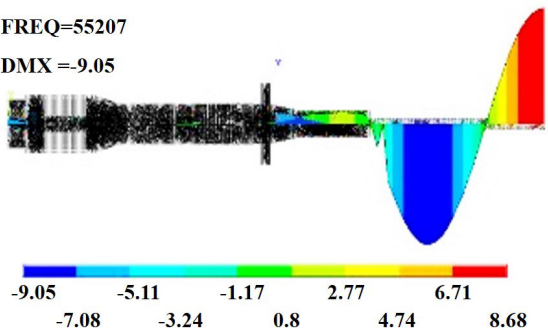


FIGURE 8. Torsional displacement distribution along the axis of the proposed enhanced hemostatic ultrasonic scalpel in modal analysis.

practically be observed only after the modified concentrator of the hemostatic ultrasonic scalpel, which indicates that the change of the working mode results from the change of the concentrator’s mechanical structure. The displacement vector distribution of the two ultrasonic scalpels has been investigated, as indicated in Figs.9 and 10. It is evident that the enhanced hemostatic ultrasonic scalpel has obtained a greater radial displacement component on the blade, which will lead to more lateral radiation energy and an enhanced ability to seal the vessel.

The results of the harmonic response analysis of the two scalpels with a driving sinewave signal with the amplitude of 150V within [50, 60KHz], which is consistent with the voltage amplitude used in the subsequent experiments, have been quantitatively summarized in Table. 4. The torsional deformation of the enhanced hemostatic ultrasonic scalpel is obviously higher than that of the conventional ultrasonic scalpel, while the other dynamic properties are similar. It has been validated by the simulation that the enhanced hemostatic scalpel has obtained a larger torsional vibration amplitude

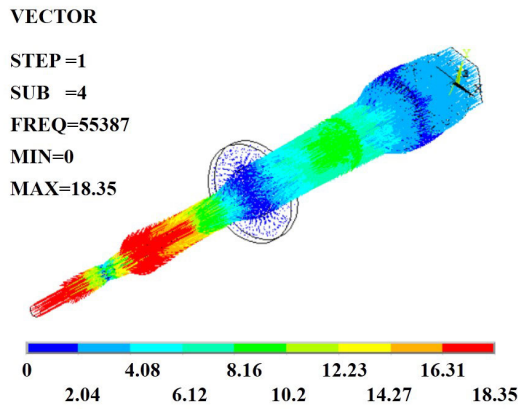


FIGURE 9. Displacement vector distribution of conventional ultrasonic scalpel.

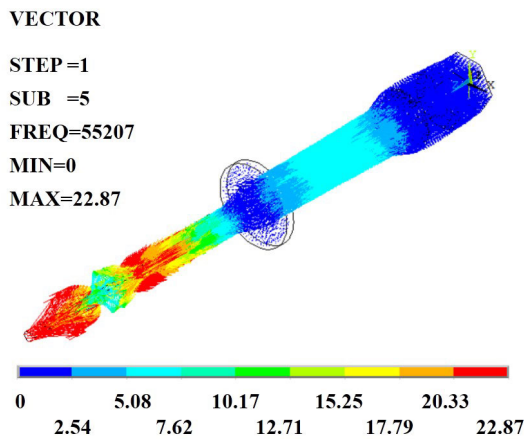


FIGURE 10. Displacement vector distribution of the proposed enhanced hemostatic ultrasonic scalpel.

TABLE 4. Performance comparison between the conventional ultrasonic scalpel and the proposed hemostatic ultrasonic scalpel.

Parameters	Conventional ultrasonic scalpel	Proposed hemostatic ultrasonic scalpel
Torsional deformation(μm)	0.0225	39.9
Axial deformation (μm)	93.6	96.3
Working frequency (kHz)	55.387	55.207

while maintaining the cutting performance after the theoretical calculation and optimization.

IV. EXPERIMENTS AND RESULTS

A. PROTOTYPE OF THE PROPOSED SCALPELS AND PERFORMANCE INVESTIGATION

The prototypes of the proposed ultrasonic scalpel and conventional ultrasonic scalpel were fabricated by computerized numerical control (CNC)-based techniques, as shown in Fig. 11. Both ultrasonic scalpels utilized the same piezoelectric converter and blade, except for the concentrator part. The dynamic parameters of both ultrasonic scalpels have been measured by an impedance analyzer (PV520A from Bandera, China) within the sweep frequency range of [50, 60KHz],

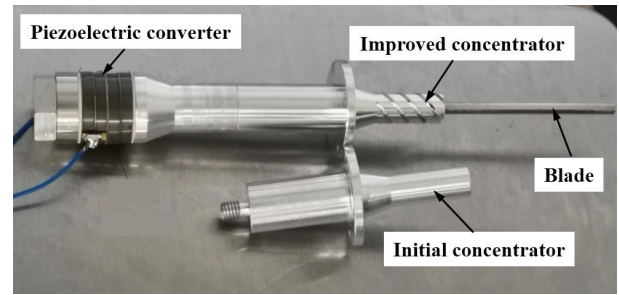


FIGURE 11. The fabricated prototypes of the designed hemostatic ultrasonic scalpel and conventional ultrasonic scalpel.

TABLE 5. Comparison of experimental parameters between the proposed ultrasonic scalpel and conventional ultrasonic scalpel.

Parameters	Conventional ultrasonic scalpel	Proposed hemostatic ultrasonic scalpel
Working frequency (Hz)	55227.7	55303.5
Equivalent resistance (Ω)	63.8	55.8
Electromechanical coupling coefficient	0.1006	0.1013
Mechanical quality factor	1335.7	1510.5

as summarized in Table. 5. The enhanced hemostatic scalpel had a similar operating frequency, and electromechanical coupling coefficients, and a decreased equivalent resistance value compared to the conventional scalpel. These results indicate that the proposed scalpel has maintained the dynamic performances while introducing the torsional vibration into longitudinal vibration. The resonance frequency of each ultrasonic scalpel only has a deviation of less than 0.5% from the target frequency, indicating the design method's effectiveness. Meanwhile, the mechanical quality factor (QF) of the hemostatic ultrasonic scalpel has achieved 1510.5, far exceeding 1000. This advantage supports an excellent efficiency of converting electrical energy into mechanical energy and enables the scalpel to generate sufficient energy for cutting.

B. EXPERIMENTAL SETUP OF THE VERTICAL TEMPERATURE DISTRIBUTION TEST

When sealing the thicker blood vessels, it is necessary to heat and coagulate deeper tissues to enhance the hemostatic effect. A desirable hemostatic performance corresponds to a better heat transfer efficiency to deeper tissues. To verify the designed ultrasonic scalpel obtains an enhanced ability in transferring heat to deeper tissues compared to the conventional ultrasonic scalpel, the vertical temperature distribution experiment was conducted. The experimental setup has been configured as shown in Fig. 12. It mainly consisted of a digital waveform generator (33500B from Keysight, China), a power amplifier (9200A from Tabor electronics, Israel) with an accuracy of $\pm 2\%$, the ultrasonic scalpels, three thermocouple probes (WRNT-01, Kaipusen, China), and a thermometer (DT-3891G, CEM, China). The waveform generator produced a sinewave with an amplitude of 3V and a

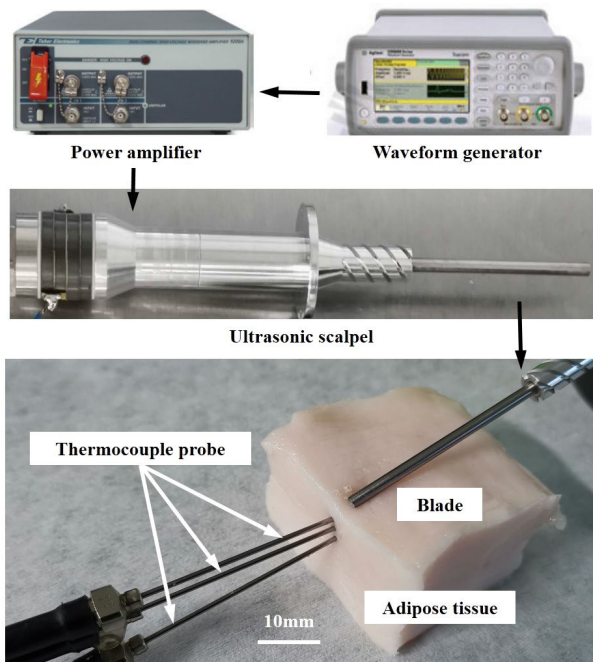


FIGURE 12. Experimental setup of the vertical temperature distribution of the adipose tissue.

frequency consistent with the scalpel’s resonance frequency. The power amplifier amplified the voltage by 50 times to provide sufficient driving power. The amplified signals were applied to the piezoelectric converter, driving the ultrasonic scalpel to transmit energy to the tissue. The subcutaneous adipose tissue of pig was chosen as the experimental target, as it is more uniform and easier to operate than the other tissues, facilitating the even transfer of heat.

The vertical temperature distribution on the tissue was measured by the thermocouple probes and recorded by the thermometer. Three thermocouple probes were utilized to measure the adipose tissue’s temperature distribution at the depth of 3mm, 6 mm and 9 mm below the tissue upper surface. For each scalpel, four measurements were carried out to reveal the heat transmission capacity, and the temperature-time relationship curves were fitted with a quintuple polynomial using the polyfit function in MATLAB. One typical group result has been shown in Fig. 13. The L-T curves (the three full lines) denote the temperature-time relationship when using the longitudinal-torsional ultrasonic scalpel, the L curves (the three dotted lines) are produced using the conventional longitudinal ultrasonic scalpel. The thin lines are the original data while the thick lines are the fitted curve. The detailed four group results of the four measurements have been summarized in Table 6. The results indicate the improved ultrasonic scalpel can generate more heat at three different depths: 24.0% higher on the 3mm layer, 16.5% higher on the 6mm layer, and 8.5% higher on the 9mm layer. Such improved outcomes validate the enhanced hemostatic ultrasonic scalpel has obtained an enhanced heat transferring capacity due to the torsional vibration component for facilitating the energy transmission.

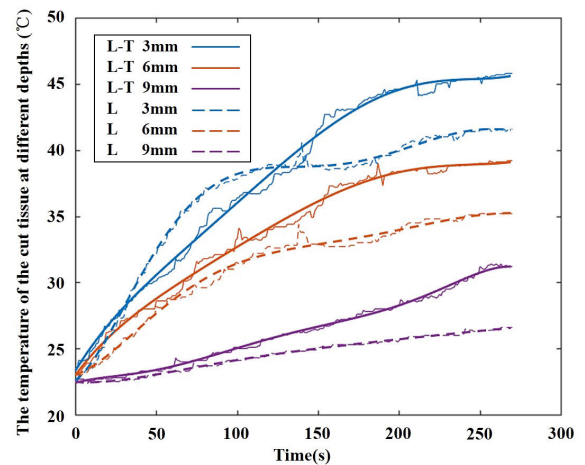


FIGURE 13. The vertical temperature distribution curves along the adipose tissue.

TABLE 6. The temperature distribution at different depths.

Parameters	1	2	3	4	Mean
L-T-3mm(°C)	54.4	49.9	48.4	56.5	52.3
L-3mm(°C)	37.6	43.9	43.6	43.5	42.2
L-T-6mm(°C)	35.3	32.3	39.9	34.1	35.4
L-6mm(°C)	32.7	27.0	35.4	26.5	30.4
L-T-9mm(°C)	26.3	23.9	29.6	23.5	25.8
L-9mm(°C)	23.3	21.8	26.6	23.7	23.8

While it can be observed that the temperature curve of the conventional scalpel in 3mm depth rises rapidly at the beginning stage, and then rises with a slow rate, the corresponding temperature curve of the improved scalpel steadily rises and then surpasses the heat increase of the conventional scalpel at some specific points for all the measured group data. This occurs because the heat of pure longitudinal vibration is mainly caused by the friction between the tissue and the blade. The friction can result in a steep increase of the blade temperature and transfers more heat to the shallow tissue in a short time, but then this increment will slow down with the time increases.

C. EX-VIVO COAGULATION DISSECTION AND BURST PRESSURE TEST EXPERIMENT ON CHICKEN CAROTID

The ex-vivo coagulation dissection and burst pressure test experiments on the chicken carotids were carried out to assess the cutting and sealing capacity of the improved ultrasonic scalpel. Plenty of chicken carotids were manually prepared and measured as shown in Fig. 14. Twenty of the carotids with diameters of 3-4mm were sifted out and equally divided into two groups. Ten dissections were conducted by the two scalpels respectively, and the corresponding burst pressure values were measured and recorded to characterize the coagulation capacity of different scalpels.

As shown in Fig. 15, the experimental setup included an infusion syringe pump (AMK321, AMK, China), a manometer (RS232, AZ Instrument Corp, Taiwan), a medical tee

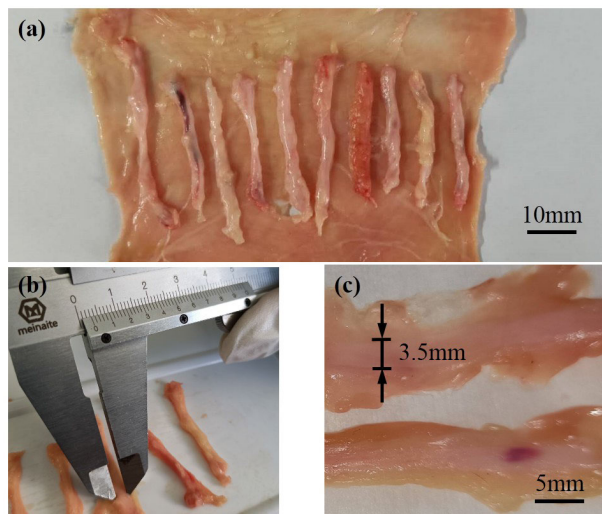


FIGURE 14. (a) Part of the prepared chicken carotids. (b) and (c) shows how the vessels were measured.

tube, and a disposable intravenous infusion tube. The infusion syringe pump was utilized to provide a stable injection speed while injecting the normal saline into the sealed vessel through a disposable intravenous infusion tube. Connected by the medical tee tube, the pump, the manometer and the sealed vessel shared the same pressure, thus the manometer can measure and record the pressure variation in the sealed vessel in real-time. One typical pressure curve has been collected, as illustrated in Fig. 16. The injection procedure started at 17s, and the vessel burst and a steep drop in pressure can be observed at about 65s along the curve. The corresponding peak pressure value was recorded as the burst pressure value for each sealed vessel. Another local peak can be found during the 20-40s injection. This happened because a certain pressure was needed to overcome the adhesive force inside the vessel in the duration of injection. Once this pressure value was sufficiently high, the inner wall of the vessel will be separated from adhesion, which also led to a sudden volume increase and a subsequent slight pressure decreases.

The burst pressure values of each group have been summarized in Table 7. The group1 was operated by the enhanced hemostatic scalpel while the group2 was produced by the conventional one. The average burst pressure value for the proposed scalpel is 12.5% higher than the conventional scalpel. If the maximum and minimum values are removed to minimize the impact of accidental circumstances on results, the trimmed mean of each group is 297.5mmHg and 247.5mmHg respectively. Then, the average burst pressure increasement rises from 12.5% to 20.2%, which denotes an improved coagulation ability. One of the recorded burst pressures (the 3rd seal) in group1 is only 120mmHg, which is significantly lower than the others (about 50% lower than the second smallest value). There existed excessive fat attached around the 3rd blood vessel in group1, and such fat turned into excess oil flowing between the vessel wall and scalpel, resulting in more heat dissipation and a poor seal. The results of the

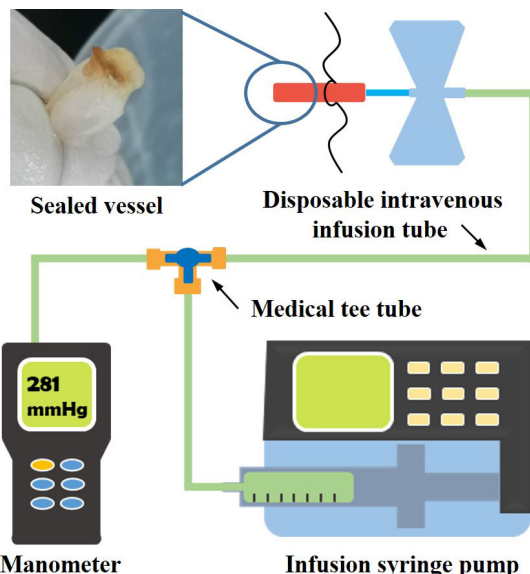


FIGURE 15. Experimental setup for investigation of the burst pressure.

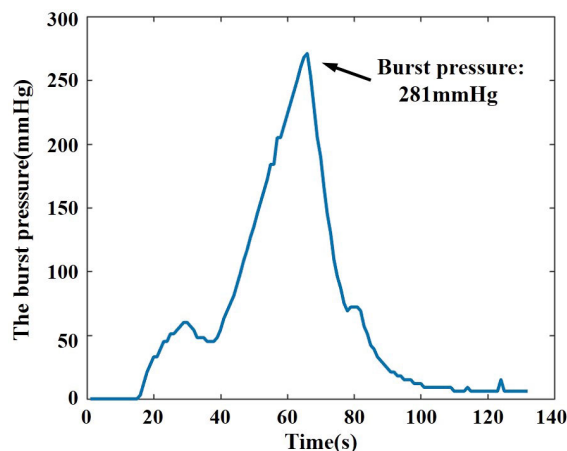


FIGURE 16. Pressure curve of the chicken carotid during the injection.

ex-vivo experiment indicate the proposed scalpel achieves an improved sealing capacity, which is well consistent with the simulation result.

D. DISCUSSION

During the experiments, we found that the resonance frequency of the ultrasonic scalpel would decrease (no more than 0.5%) with the heat generation and accumulation on the piezoelectric ceramic and the ultrasonic scalpel blade during the tissue-tool interaction. With the increase of continuous working duration, this phenomenon tends to become more apparent, which would affect the performances of the ultrasonic scalpel. It is necessary to track the resonance frequency of the ultrasonic scalpel and adjust working frequency accordingly, targeting to realize the cutting and sealing with a high efficiency [34]. For the coagulation dissection experiments of chicken carotids, it is worth noting that the excessive

TABLE 7. The burst pressure values of each group.

Parameters	Group1(mmHg)	Group2(mmHg)
1	281	163
2	286	169
3	120	271
4	281	275
5	250	245
6	347	178
7	465	225
8	326	492
9	398	382
10	211	235
Mean	296.5	263.5
Trimmed Mean	297.5	247.5

fat attached to the vessels is harmful to the sealing effect. A proper surface modification of the blade that can be investigated with the bioinspired design to realize fast drain of the generated oil, should be effective to avoid such phenomenon and further improve the sealing ability [35].

V. CONCLUSION

The theoretical design, structural optimization, dynamic analysis, and experimental tests of the enhanced hemostatic ultrasonic scalpel have been presented in this paper. The electromechanical equivalent method was employed to determine the initial geometric dimensions of the scalpels. The specific design with four spiral grooves on the concentrator changes the working mode from the longitudinal vibration to the longitudinal-torsional vibration. The vertical motion component is enlarged correspondingly, facilitating the energy transmission to enhance the sealing capacity. The FEM-based simulation was carried out to perform simulation and design optimization to further improve the scalpel's cutting and sealing performances. The temperature distribution experiments on subcutaneous adipose tissue were conducted to validate the improved heat transferring efficiency. The proposed ultrasonic scalpel achieved better results than that of the conventional scalpel at different tissue layers. The sealing capacity of the ultrasonic scalpels has been investigated through the coagulation dissection and burst pressure test of the chicken carotid experiment. The improved average burst pressure value has verified the enhanced hemostatic effects of the proposed ultrasonic scalpel. Future work will involve the implementation of the frequency tracking technique to design the driving part and further improve the cutting and coagulation performances, and the application of Fiber Bragg Grating-based force and temperature sensing to monitor the operational process [36]. The assessment of thermal damage and comparison with other kinds of ultrasonic scalpels will be also investigated.

REFERENCES

- [1] D. Dutta and I. Dutta, "The harmonic scalpel," *J. Obstetrics Gynecol. India*, vol. 66, no. 3, pp. 209–210, Jun. 2016.
- [2] T. A. Emam and A. Cuschieri, "How safe is high-power ultrasonic dissection?" *Ann. Surg.*, vol. 237, no. 2, pp. 186–191, Feb. 2003.
- [3] P. A. Sutton, S. Awad, A. C. Perkins, and D. N. Lobo, "Comparison of lateral thermal spread using monopolar and bipolar diathermy, the harmonic scalpel (TM) and the ligasure (TM)," *Brit. J. Surg.*, vol. 97, no. 3, pp. 428–433, Mar. 2010.
- [4] C. Choi, I. G. Do, and T. Song, "Ultrasonic versus monopolar energy-based surgical devices in terms of surgical smoke and lateral thermal damage (ULMOST): A randomized controlled trial," *Surgical Endoscopy*, vol. 32, no. 11, pp. 4415–4421, Apr. 2018.
- [5] L. F. Grochola and R. Vonlanthen, "Surgical energy devices or devices for hemostasis," in *Atlas of Upper Gastrointestinal and Hepato-Pancreato-Biliary Surgery*, vol. 6. Springer, 2016, pp. 37–44.
- [6] C. Shi, D. K. Luu, Q. Yang, J. Liu, J. Chen, C. Ru, S. Xie, J. Luo, J. Ge, and Y. Sun, "Recent advances in nanorobotic manipulation inside scanning electron microscopes," *Microsystems Nanoeng.*, vol. 2, no. 1, pp. 1–16, Jun. 2016.
- [7] F. Wang, C. Liang, Y. Tian, X. Zhao, and D. Zhang, "Design of a piezoelectric-actuated microgripper with a three-stage flexure-based amplification," *IEEE/ASME Trans. Mechatronics*, vol. 20, no. 5, pp. 2205–2213, Oct. 2015.
- [8] G. Gu, L. Zhu, C. Su, H. Ding, and S. Fatikow, "Modeling and control of piezo-actuated nanopositioning stages: A survey," *IEEE Trans. Autom. Sci. Eng.*, vol. 13, no. 1, pp. 313–332, Jan. 2016.
- [9] C. Shi, X. Dong, and Z. Yang, "A microgripper with a large magnification ratio and high structural stiffness based on a flexure-enabled mechanism," *IEEE/ASME Trans. Mechatronics*, to be published.
- [10] S. Lin, "Radial vibration of the composite ultrasonic transducer of piezoelectric and metal rings," *IEEE Trans. Ultrason., Ferroelectr., Freq. Control*, vol. 54, no. 6, pp. 1276–1280, Jun. 2008.
- [11] A. Abdullah, M. Shahini, and A. Pak, "An approach to design a high power piezoelectric ultrasonic transducer," *J. Electroceram.*, vol. 22, no. 4, pp. 369–382, Jun. 2009.
- [12] T. Ogawa, R. Hattori, T. Yamamoto, and M. Gotoh, "Safe use of ultrasonically activated devices based on current studies," *Expert Rev. Med. Devices*, vol. 8, no. 3, pp. 319–324, Jun. 2011.
- [13] S. S. Ching and M. J. McMahon, "Comparison of linear and torsional mode ultrasonic coagulating shears for the sealing of medium-to large-sized arteries," *Surgical Endoscopy*, vol. 21, no. 7, pp. 1165–1169, Jun. 2007.
- [14] J. Landman, K. Kerbl, J. Rehman, C. Andreoni, P. A. Humphrey, W. Collyer, E. Olweny, C. Sundaram, and R. V. Clayman, "Evaluation of a vessel sealing system, bipolar electro-surgery, harmonic scalpel, titanium clips, endoscopic gastrointestinal anastomosis vascular staples and sutures for arterial and venous ligation in a porcine model," *J. Urol.*, vol. 169, no. 2, pp. 697–700, Feb. 2003.
- [15] S. C. Wong, W. Bachinsky, P. Cambier, R. Stoler, J. Aji, J. H. Rogers, J. Hermiller, R. Nair, H. Hutman, and H. Wang, "A randomized comparison of a novel bioabsorbable vascular closure device versus manual compression in the achievement of hemostasis after percutaneous femoral procedures," *JACC, Cardiovascular Interventions*, vol. 2, no. 8, pp. 785–793, Aug. 2009.
- [16] S. Wang, J. Wang, and J. Li, "Modelling and quality control of robot-assisted gastrointestinal assembly," *CIRP Ann.*, vol. 64, no. 1, pp. 21–24, 2015.
- [17] J. Clymer, R. Timm, K. Tellio, A. Welling, R. Asher, and J. Amaral, "Sealing vessels up to 7 mm in diameter solely with ultrasonic technology," *Med. Devices*, vol. 7, pp. 263–271, Jul. 2014.
- [18] Z. Pogorelić, Z. Perko, N. Družijanić, S. Tomić, and I. Mrklić, "How to prevent lateral thermal damage to tissue using the harmonic scalpel: Experimental study on pig small intestine and abdominal wall," *Eur. Surgical Res.*, vol. 43, no. 2, pp. 235–240, Oct. 2009.
- [19] A. Henderson, E. Whitehead, M. Nora, and A. Rane, "LOTUS vs. Harmonic scalpel: A controlled pilot study of efficacy ergonomics and pathological outcome in the porcine model," *Urology*, vol. 68, p. 22, Nov. 2006.
- [20] J. Milsom, K. Trencheva, S. Monette, R. Pavor, P. Shukla, J. Ma, and T. Sonoda, "Evaluation of the safety, efficacy, and versatility of a new surgical energy device (THUNDERBEAT) in comparison with harmonic ACE, LigaSure V, and EnSeal devices in a porcine model," *J. Laparoendoscopic Adv. Surgical Techn.*, vol. 22, no. 4, pp. 378–386, May 2012.
- [21] G. Ogura, R. Nakamura, Y. Muragaki, M. Hashizume, and H. Iseki, "Development of an articulating ultrasonically activated device for Laparoscopic surgery," *Surgical Endoscopy*, vol. 23, no. 9, pp. 2138–2142, Sep. 2009.
- [22] I. Khalaji, M. D. Naish, and R. V. Patel, "Articulating minimally invasive ultrasonic tool for robotics-assisted surgery," in *Proc. IEEE Int. Conf. Robot. Autom. (ICRA)*, Seattle, WA, USA, May 2015, pp. 573–578.

[23] Y. Kuang, M. Sadiq, S. Cochran, and Z. Huang, "Design and characterization of an ultrasonic surgical tool using d₃₁ PMN-PT plate," *Phys. Procedia*, vol. 63, pp. 182–188, Dec. 2015.

[24] K. Ebina, H. Hasegawa, and H. Kanai, "Investigation of frequency characteristics in cutting of soft tissue using prototype ultrasonic knives," *Jpn. J. Appl. Phys.*, vol. 46, no. 7, pp. 4793–4800, Jul. 2007.

[25] L. Zheng, Z. Xu, L. Yuan, and Z. Peng, "Study on vibration frequency optimization of ultrasonic scalpel," *China Med. Equip.*, vol. 33, no. 5, pp. 62–65, Jun. 2018.

[26] S. Y. Lin, *The Principle and Design of Ultrasonic Transducers*. Beijing, China: Science Press, Jun. 2004.

[27] H. J. Rack and J. I. Qazi, "Titanium alloys for biomedical applications," *Mater. Sci. Eng. C*, vol. 26, no. 8, pp. 1269–1277, Sep. 2006.

[28] F. Wang, X. Zhao, D. Zhang, and Y. Wu, "Development of novel ultrasonic transducers for microelectronics packaging," *J. Mater. Process. Technol.*, vol. 209, no. 3, pp. 1291–1301, Feb. 2009.

[29] X. Dong, K. Uchino, C. Jiang, L. Jin, Z. Xu, and Y. Yuan, "Electromechanical equivalent circuit model of a piezoelectric disk considering three internal losses," *IEEE Access*, vol. 8, pp. 181848–181854, Oct. 2020.

[30] P. Harkness, A. Cardoni, and M. Lucas, "Ultrasonic rock drilling devices using longitudinal-torsional compound vibration," in *Proc. IEEE Int. Ultrason. Symp.*, Rome, Italy, Sep. 2009, pp. 2088–2091.

[31] R. Cleary and M. Lucas, "Comparison of longitudinal-mode and Longitudinal-torsional mode ultrasonic bone biopsy devices," in *Proc. IEEE Int. Ultrason. Symp. (IUS)*, Kobe, Japan, Oct. 2018.

[32] F. Wang, H. Zhang, C. Liang, Y. Tian, X. Zhao, and D. Zhang, "Design of high-frequency ultrasonic transducers with flexure decoupling flanges for thermosonic bonding," *IEEE Trans. Ind. Electron.*, vol. 63, no. 4, pp. 2304–2312, Apr. 2016.

[33] C. Shi, M. Li, C. Lv, J. Li, and S. Wang, "A high-sensitivity fiber Bragg grating-based distal force sensor for Laparoscopic surgery," *IEEE Sensors J.*, vol. 20, no. 5, pp. 2467–2475, Mar. 2020.

[34] H. Zhang, F. Wang, D. Zhang, L. Wang, Y. Hou, and T. Xi, "A new automatic resonance frequency tracking method for piezoelectric ultrasonic transducers used in thermosonic wire bonding," *Sens. Actuators A, Phys.*, vol. 235, pp. 140–150, Nov. 2015.

[35] H. Chen, T. Ran, Y. Gan, J. Zhou, Y. Zhang, L. Zhang, D. Zhang, and L. Jiang, "Ultrafast water harvesting and transport in hierarchical microchannels," *Nature Mater.*, vol. 17, no. 10, pp. 935–942, Oct. 2018.

[36] C. Lv, S. Wang, and C. Shi, "A high-precision and miniature fiber Bragg grating-based force sensor for tissue palpation during minimally invasive surgery," *Ann. Biomed. Eng.*, vol. 48, no. 2, pp. 669–681, Feb. 2020.



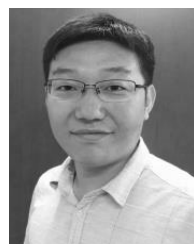
XINYU DONG received the B.Eng. degree in mechanical engineering from the School of Mechanical Engineering, Yanshan University, Qinhuangdao, China, in 2018. He is currently pursuing the master's degree in mechanical engineering with the School of Mechanical Engineering, Tianjin University, Tianjin, China. His current research interest includes flexure mechanism design and control.



GUANGHAO ZHANG received the B.Eng. degree in mechanical engineering from the School of Mechanical Engineering, Shandong University, Jinan, China, in 2020. He is currently pursuing the master's degree in mechanical engineering with the School of Mechanical Engineering, Tianjin University, Tianjin, China. His current research interest includes flexure mechanism design and control.



ZHICHENG GUO received the B.Eng. degree in mechanical engineering from the School of Mechanical Engineering, Yanshan University, Qinhuangdao, China, in 2017, and the master's degree in mechanical engineering from the School of Mechanical Engineering, Tianjin University, Tianjin, China, in 2019.



GUOKAI ZHANG received the B.S. and Ph.D. degrees from the Department of Mechanical Engineering, Tianjin University, China, in 2011 and 2018, respectively.

He is currently a Research Associate with the School of Biomedical Engineering and Imaging Sciences, King's College London, London, U.K. His research interests include analysis of soft transmission systems, design and optimization of surgical robot systems, and NOTES device.



JINHUA LI (Member, IEEE) received the B.Eng. degree in automation and the M.S. degree in control theory and control engineering from Tianjin Polytechnic University, China, in 1996 and 1999, respectively, and the Ph.D. degree in engineering from Yamaguchi University, Japan, in 2005. Since October 2007, he has been an Associate Professor of Mechanical Engineering with Tianjin University, China. His current research interest includes control theory and

its applications to surgical robots.



CHAOYANG SHI (Member, IEEE) received the Ph.D. degree from the Department of Micro-Nano Systems Engineering, Nagoya University, Nagoya, Japan, in 2013. He was a Postdoctoral Research Fellow with Imperial College London, U.K., and the University of Toronto, Toronto, ON, Canada. He is currently a Professor with the School of Mechanical Engineering, Tianjin University. His research interests include medical robotics, micro-nano robotics, and FBG-based sensing techniques.

• • •